1 **Title**

2 Type I interferon responses contribute to immune protection against mycobacterial infection

3 **Authors**

4 Andrea Szydlo-Shein[1], Blanca Sanz-Magallón Duque de Estrada[1], Joshua Rosenheim[1], Carolin T.
5 Turner[1], Evdokia Tsaliki[1], Marc C. I. Lipman[2,3], Heinke Kunst[4,5], Gabriele Pollara[1], Philip M. Elks[6],
6 Jean-Pierre Levraud[7], Elspeth M. Payne[8], Mahdad Noursadeghi[1], Gillian S. Tomlinson[1]*

7 **Affiliations**

8 [1]Division of Infection and Immunity, University College London, London, UK

9 [2]Respiratory Medicine, Royal Free London NHS Foundation Trust, London, UK

10 [3]UCL Respiratory, University College London, London, UK

11 [4]Barts Health NHS Trust, London, UK

12 [5]Blizard Institute, Queen Mary University of London, London, UK

13 [6]The Bateson Centre, School of Medicine and Population Health, The University of Sheffield,
14 Sheffield, UK

15 [7]Université Paris-Saclay, CNRS UMR9197, Institut Pasteur, Université Paris-Cité, Institut des
16 Neurosciences Paris-Saclay, 91400 Saclay, France

17 [8]Research Department of Haematology, Cancer Institute, University College London, London, UK

18 *Corresponding author

19 **Corresponding author**

20 Gillian S. Tomlinson, Email: g.tomlinson@ucl.ac.uk

21

ABSTRACT

Reasons for the spectrum of severity of active tuberculosis (TB) disease are incompletely understood. We sought to identify master regulators of host immune responses that determine disease severity in pulmonary TB. We performed molecular profiling of human in vivo immune responses to discover associations with the extent of radiographic TB disease in a patient cohort. We then undertook mechanistic studies to test causality for the observed associations using the zebrafish larval *Mycobacterium marinum* infection model. Transcriptional profiling of human immune recall responses to tuberculin skin test (TST) challenge, a surrogate for immune responses to TB in the lung, revealed that type I interferon activity in the TST transcriptome was inversely associated with radiological disease severity. Abrogation of type I interferon signalling, achieved by CRISPR-mediated mutagenesis of *stat2*, led to increased susceptibility of zebrafish larvae to *M. marinum* infection, as a result of reduced recruitment of myeloid cells required to restrict mycobacterial growth, to the site of disease. Our data support a host protective role for type I interferon responses in mycobacterial infection, with potential applications for risk-stratification of adverse outcomes and development of a host-directed therapy to mitigate against severe disease.

ONE SENTENCE SUMMARY

Type I interferon responses contribute to host immune protection in mycobacterial infection by recruitment of myeloid cells to the site of disease.

INTRODUCTION

Mycobacterium tuberculosis (Mtb) infection results in diverse clinical manifestations, ranging from asymptomatic infection to active tuberculosis (TB), which comprises an enormous spectrum of disease severity *(1, 2)*. Although we know that immune responses contribute to the risk of disease, current understanding of the role of immune response variation in disease severity is limited. Identification of immune correlates of disease severity may offer new insights into the immune pathways that contribute to protection and pathogenesis. This is necessary to enable novel vaccine design and evaluation, stratify disease risk in people who become infected and inform development of novel host-directed therapies to shorten treatment regimens, mitigate against antimicrobial resistance, and against the chronic sequelae of tissue injury in TB *(3)*.

Variation in tissue immunology of human TB at the site of established disease is likely confounded by differences in the chronicity of the disease process. To overcome this limitation, we evaluated in vivo immune responses at the site of a standardised antigenic challenge using the tuberculin skin test (TST). We have previously shown that transcriptional profiling of skin biopsies from the site of the TST provides comprehensive molecular and systems level evaluation of human in vivo immune responses to Mtb with significantly greater sensitivity than conventional clinical and histological assessments *(4, 5)*. The TST gene signature is enriched within pulmonary TB granulomas and accounts for genome-wide differences in the transcriptomes of TB infected lung compared to healthy lung tissue *(5, 6)*. Therefore, the TST provides a faithful and readily accessible surrogate to study immune responses at the site of TB disease.

In the present study, we identified quantitative variation in immune pathways in the TST response correlated with the severity of human TB disease, and then tested the hypothesis that these pathways were causally related to outcomes of *Mycobacterium marinum* infection in zebrafish larvae. This natural host-pathogen interaction generates granulomatous inflammation that recapitulates key aspects of human TB pathology and in particular, provides unparalleled opportunities to study innate immune responses in isolation, given the absence of functional adaptive immunity until 3-4 weeks *(7)*. Our innovative strategy revealed an inverse relationship between type I interferon activity and radiographic severity of human TB, suggesting a host-protective role for type I interferons, that we confirmed in zebrafish larvae by showing that mutagenesis of *stat2* to model abrogation of downstream type I interferon signalling led to increased severity of *M. marinum* infection.

RESULTS

Outlier analysis of the TST transcriptome defines human in vivo immune responses to active tuberculosis

We supplemented data from our previously reported TST transcriptional responses *(8)* to provide a total sample size of 51 people with microbiologically confirmed pulmonary TB who were within one month of commencing anti-tuberculous chemotherapy (Table 1, Fig. S1A, B). We evaluated disease severity using a published radiographic scoring system which incorporates extent of disease and the presence of cavitation on chest x-ray *(9)*. In order to capture the inter-individual variation in immune response to the mycobacterial challenge, outlier profile analysis *(10)* was used to identify transcripts in the TST of each individual that were significantly enriched compared to gene expression in control data from skin biopsies at the site of saline injections. The integrated list of outlier genes statistically enriched in TST samples compared to control saline samples from all 51 individuals defined an active TB TST transcriptome comprised of 3222 transcripts. This analysis revealed that although some aspects of the TST response are consistent in all people, there is also considerable variability between individuals (Fig. S1C). The 3222 transcripts identified by this approach, were enriched for canonical pathways involved in cell mediated responses, consistent with our previous description of the TST gene signature identified by conventional differential gene expression analysis *(5, 8)* (Fig. S1D).

Reduced type I interferon activity in the TST transcriptome is associated with increased severity of human TB disease

Next, we sought to identify immunological pathways correlated with disease severity. We identified individual genes in the TST transcriptome that showed statistically significant correlations with the

radiographic severity score. We subjected these genes to Ingenuity Pathway Analysis upstream regulator analysis to collate groups of co-regulated genes (Fig. 1A and Fig. S2A). These were annotated by their upstream regulators at the level of cytokines, transmembrane receptors, kinases and transcriptional regulators, representing the key components of signalling pathways which mediate immune responses. To provide increased confidence that these modules represented co-regulated genes in each molecular pathway, we retained only those that had significantly greater co-correlated expression than modules of genes randomly selected from our TST transcriptomes *(11)*. 111 modules were identified among genes inversely correlated with radiographic TB severity, suggesting they may contribute to host protection against severe disease (Fig. 1A-C and Fig. S2B). These included transcriptional modules representing pro-inflammatory cytokine activity (tumour necrosis factor alpha and interleukin (IL)1 beta), interferon gamma and T cell activity, consistent with existing evidence predominantly supporting their protective roles in TB *(12)* (Fig. 1B). In addition, we found enrichment of multiple co-regulated gene networks attributed to type I interferon signalling, suggesting that type I interferon responses may also contribute to host protection in mycobacterial infection (Fig. 1B, C). Interferon gamma was also predicted to regulate one of only two small putative networks within genes positively correlated with disease severity; the other driven by TCL1A, an AKT kinase activator that promotes cellular survival *(13)* (Fig. S2C).

To validate the immunological responses predicted to be associated with disease severity by upstream regulator analysis, we quantified the expression of two independently derived and largely non-overlapping type I interferon inducible gene modules reflecting the biological activity of type I interferons (Table S1) *(5, 8)*, within the TB TST transcriptome (Fig. 1D). This provided independent validation of the inverse relationship between type I interferon responses and radiographic severity of TB (Fig. 1E), suggestive of a host-protective role. By contrast, the expression of the entire TST transcriptome and that of three distinct independently derived interferon gamma inducible gene modules *(5)* (Table S1) did not correlate with disease severity (Fig. S3).

stat2 CRISPant zebrafish larvae exhibit increased susceptibility to *M. marinum* infection

The TST transcriptome does not solely reflect anti-mycobacterial T cell memory *(4)* and type I interferons are primarily induced following activation of innate immune recognition pathways *(14)*. Therefore, to evaluate whether impaired type I interferon responses cause more severe mycobacterial disease, we exploited the zebrafish larval *M. marinum* infection model, which allows exclusive assessment of innate immunity *(7)*. The mammalian canonical type I interferon signalling pathway is highly conserved in zebrafish *(15, 16)* (Fig. 2A). First, we confirmed that intravenous *M. marinum* infection of wild type zebrafish larvae induces a type I interferon response, as evidenced by enrichment for two distinct independently derived transcriptional modules reflecting type I interferon activity *(11, 16)* (Table S1) within genome-wide transcriptomic data obtained after four days of mycobacterial growth (Fig. 2B, C). To block downstream type I interferon signalling we used CRISPR-mediated mutagenesis of *stat2*, a subunit of the interferon stimulated gene factor (ISGF)3, the principal transcription factor complex which induces expression of type I interferon stimulated genes (ISG) *(17–19)*, for which there is a single zebrafish orthologue *(15)* (Fig. 2A). Injection of three guide RNA/Cas9 ribonucleoprotein (RNP) complexes each targeting a distinct *stat2* exon, into one cell stage wild type zebrafish embryos led to >90% efficient mutagenesis, confirmed by next-generation sequencing (Fig. S4A and Fig. S5A). We verified loss of functional downstream type I interferon signalling by showing that induction of the classical ISG Mxa *(16, 19)* by recombinant interferon phi 1, measured by expression of a reporter *mxa:mCherry* transgene, was significantly attenuated in *stat2* CRISPants compared to siblings injected with “scrambled” (negative control) RNPs designed to lack genomic targets (Fig. S4B and Fig. S5B-C). *stat2* CRISPants developed normally up to five days post-fertilisation (Fig. S5B).

There was no difference in survival of *M. marinum* infected *stat2* CRISPants and scrambled RNP injected siblings (Fig. 3A, B) within the timeframe of our experiments. However, mycobacterial burden, the number of bacterial foci and the spatial dissemination of bacteria, determined by quantitation of fluorescent foci of *M. marinum*, were all significantly higher in intravenously infected *stat2* CRISPants compared to control RNP injected siblings, indicative of more severe disease (Fig. 3A, C-E). These findings are consistent with a host protective role for type I interferons in mycobacterial infection, as suggested by our observation of an association between reduced type I interferon activity and increased disease severity in human TB (Fig. 1).

Steady state neutrophil numbers are reduced in *stat2* CRISPant zebrafish larvae

Macrophages are critically important for control of *M. marinum* infection in zebrafish larvae *(20–22)* and neutrophils may also contribute to mycobacterial killing *(23, 24)*. Therefore, to investigate the mechanisms by which *stat2* deficiency leads to worse mycobacterial infection we used transgenic zebrafish lines with fluorescent immune cell lineages to generate *stat2* CRISPants that have fluorescent macrophages or neutrophils. First, we asked whether *stat2* disruption impacted steady state macrophage or neutrophil numbers. We demonstrated by quantitative fluorescence microscopy, using integrated fluorescence as a surrogate for cell number, that *stat2* deficiency did not affect baseline macrophage numbers (Fig. 4A, B). However, it was associated with reduced neutrophil numbers (Fig. 4C, D).

Recruitment of macrophages but not neutrophils to the site of sterile injury is *stat2* dependent

Type I interferons have previously been shown to influence cellular migration *(14, 25)*. Therefore, we tested macrophage and neutrophil recruitment in *stat2* CRISPants using a tailfin transection model of sterile injury, most commonly used to evaluate neutrophil recruitment *(26)* (Fig. S4C). The timing of neutrophil homing to the site of sterile tail fin transection was normal in *stat2* CRISPants, with maximal accumulation at six hours and dissipation of recruited cells becoming evident by 24 hours, similar to that of control RNP injected embryos (Fig. 5A, B) and in keeping with previous studies *(26, 27)*. Despite baseline neutropenia, the number of neutrophils at the wound site at the point of maximal recruitment in *stat2* CRISPants exceeded that of control RNP injected embryos. But by 24 hours the number of neutrophils at the injury site was significantly reduced in *stat2* CRISPants, likely reflecting the attenuated increase in total neutrophil numbers in response to the acute inflammatory challenge (Fig. 5C, D).

As previously reported, macrophage recruitment to the tail wound site was slower than that of neutrophils *(27, 28)*. Very few macrophages were present at the tailfin transection site by one hour in either *stat2* disrupted or control transgenic larvae, but recruitment progressively increased until 24 hours in both groups (Fig. 6). Fewer macrophages were found in the vicinity of the wound site at all time points post-injury in *stat2* CRISPant transgenic embryos compared to control RNP injected siblings, the majority being located outwith the tailfin (Fig. 6). Taken together these data suggest that *stat2* is necessary for macrophage recruitment but non-essential for neutrophil recruitment to a sterile injury site. In addition, baseline neutropenia did not impact the number of cells localised to the wound at peak neutrophil recruitment.

Recruitment of myeloid cells to the site of *M. marinum* infection is *stat2* dependent

Next we focused on macrophage recruitment to the site of mycobacterial infection because this has been reported to be crucial for control of *M. marinum* growth in zebrafish larvae *(21)*. We found a significant reduction in the number of macrophages recruited to the site of localised hindbrain *M. marinum* infection in *stat2* deficient transgenic zebrafish larvae compared to their counterparts injected with scrambled RNPs (Fig. S4D and Fig. 7A, B). We then evaluated whether *stat2* disruption affected recruitment of neutrophils to the site of mycobacterial infection. We found that in contrast to their normal peak recruitment to a sterile wound, the number of neutrophils attracted to the site of mycobacterial disease was also significantly diminished in *stat2* CRISPants (Fig 7C, D). Collectively, these results demonstrate that myeloid cell recruitment to the site of *M. marinum* infection is *stat2* dependent.

In total, the recruitment studies suggest that *stat2* disruption leads to a broad defect in macrophage recruitment to both infectious and non-infectious inflammatory foci. By contrast, *stat2* is non-essential for neutrophil migration to sterile injury. The latter finding is consistent with defective migration, rather than neutropenia, being the principal mechanism for reduced neutrophil numbers at the site of *M. marinum* infection.

Discussion

We have taken an innovative approach, combining molecular and systems level evaluation of human immune responses to a standardised experimental challenge, to identify master regulators of

biological pathways associated with TB disease severity. We experimentally validated host factors responsible for differences in phenotype using a relevant, tractable animal model which represents a natural host-pathogen pairing *(7)*. Molecular interrogation of human in vivo responses to Mtb revealed that reduced type I interferon activity within the TST transcriptome was associated with worse pulmonary disease. Deficient type I interferon signalling, achieved by genetic disruption of *stat2*, led to more severe mycobacterial infection in zebrafish larvae, via a mechanism involving impaired recruitment of macrophages and neutrophils to the site of disease and reduced neutrophil numbers at baseline. Taken together our results demonstrate an important role for type I interferon responses in contributing to innate immune protection against mycobacterial disease.

Peripheral blood interferon-inducible gene expression that diminishes with successful treatment is detectable in human active TB *(29–31)*. These transcriptional signatures comprise both type I and type II interferon inducible genes but have mainly been interpreted as type I interferon responses, fostering the view that type I interferons are detrimental to the host in human TB. Mouse data predominantly suggest that type I interferon responses contribute to increased susceptibility to mycobacterial infection by mechanisms including antagonism of IL1 mediated protection *(32–34)* and reduced responsiveness of macrophages to interferon gamma *(35)*. However, this phenotype has not been universally observed, likely due to differences in host and pathogen genetics *(36)*. Moreover, impaired type I interferon responses are generally associated with relatively minor differences in bacterial burden or survival *(36)*. Of note, Mtb is not a natural mouse pathogen, and this approach may not model host-pathogen interactions in human TB faithfully *(37)*.

In support of a protective role for type I interferons, adjunctive interferon alpha therapy in addition to conventional anti-tuberculous antibiotic treatment led to symptomatic and radiological improvement, with a reduction in bacterial burden in respiratory tract samples, in small-scale human studies *(38–40)*. In keeping with this, an early peripheral blood type I interferon-inducible gene signature predicts successful BCG-induced protection of macaques from subsequent Mtb challenge *(41)*. Type I interferon mediated restriction of mycobacterial growth in in vitro granulomas comprising collagen impregnated microspheres containing Mtb infected human peripheral blood mononuclear cells (PBMC) *(42)* also suggests that type I interferon responses benefit the host.

Our observation of reduced recruitment of macrophages to the site of disease is likely the most important factor driving increased susceptibility to *M. marinum* infection in *stat2* CRISPants. Although macrophages have been implicated in the dissemination of *M. marinum* in zebrafish larvae *(20, 43)*, reduction of total macrophage numbers, impaired macrophage migration to the site of mycobacterial infection or failure to control intracellular bacterial growth within macrophages have all been associated with poor outcome *(20–22, 44, 45)*. In contrast, increasing macrophage numbers via augmentation of M-CSF signalling either pre- or post-granuloma formation, promotes resistance to *M. marinum* infection by reducing granuloma necrosis, with consequent curtailment of extracellular mycobacterial growth *(21)*. The recent report that human genetically inherited CCR2 deficiency is associated with reduced pulmonary recruitment of monocytes, resulting in depleted numbers of functionally normal alveolar macrophages and increased susceptibility to mycobacteria, is also consistent with the notion that adequate numbers of macrophages are important for protective anti-mycobacterial immunity *(46)*.

The reduction in neutrophils present at the site of *M. marinum* infection in *stat2* CRISPants may have arisen due to baseline neutropenia, defective migration or both combined. On the basis that steady state neutropenia did not affect the timing and magnitude of peak neutrophil recruitment to sterile injury, impaired migration is probably the main driver of this phenotype, which likely also contributed to increased severity of mycobacterial disease. Previous data show that reduced access of neutrophils to mycobacteria leads to increased bacterial burden in a zebrafish line in which neutrophils express mutant *cxcr4*, resulting in peripheral neutropenia and impaired neutrophil recruitment to sites of inflammation, due to their retention in haematopoietic tissue *(23, 47)*.

Our study has some limitations. We were not able to address the reasons for variation in type I interferon activity in our human cohort. Serum samples for measurement of autoantibodies to type I interferons are not available and our sample size is insufficient for robust detection of associations between genetic variation and the expression levels of type I interferon signalling pathway genes. We were also unable to completely disentangle whether reduced neutrophil recruitment to the site of *M. marinum* infection was a consequence of neutropenia or impaired migration. We have not

determined the mechanism by which attenuated type I interferon signalling leads to reduced myeloid cell recruitment to *M. marinum*. The expression of several chemokines is type I interferon inducible *(25, 48, 49)* and the CCR2-CCL2 and CXCR3-CXCL11 chemokine axes are known to be involved in macrophage recruitment to *M. marinum (43, 50)*. Future studies are required to test the hypothesis that *stat2* mutagenesis disrupts chemokine-mediated cellular recruitment to the site of mycobacterial disease. Nonetheless, our work provides new insights into type I interferon mediated host protection against mycobacterial infection.

Variation in type I interferon responses may arise due to genetically or epigenetically encoded variation in the immune response to Mtb, neutralising type I interferon auto-antibodies, burden and virulence of the mycobacterial inoculum and stochasticity in the immune response pathway following exposure *(51–55)*. A central tenet of all these possibilities is that differences in the host immune response to Mtb lead to differences in disease severity. Our findings have potential implications for risk stratification of individuals in whom any of these mechanisms predisposing to low type I interferon activity are identified. In active TB, such individuals could be targeted for longer or more intensive drug regimens, or adjunctive type I interferon therapy delivered to the respiratory tract, to mitigate against severe disease. Early intervention with type I interferon treatment, before destruction of the lung parenchyma, is likely to be crucial to augment macrophage containment of Mtb, but timing and duration of therapy will require evaluation in relatively large-scale experimental medicine trials.

MATERIALS AND METHODS

Ethics statement

The study was approved by the London Bloomsbury Research Ethics Committee (16/LO/0776). Written informed consent was obtained from all participants.

Study design

We aimed to identify master regulators of human immune responses that correlate with severity of TB disease, using transcriptional profiling of biopsies from the TST as a surrogate for immune responses to TB in the lung and to test causation for observed associations by genetic manipulation of identified upstream regulator molecules in the zebrafish larval mycobacterial infection model. To encompass a broad spectrum of disease severity we recruited 51 adults (>18 years) from four London hospitals, newly diagnosed with smear or culture positive pulmonary TB, who were within four weeks of starting treatment. This is in keeping with the median sample size of previous studies which have successfully demonstrated a relationship between severity of TB disease and immunological parameters *(29, 56–59)*. Individuals with coincident human immunodeficiency virus infection, malignancy, taking immunomodulatory therapy, a history of immunization within the preceding two weeks or previous keloid formation, or unable to give informed consent were excluded. Study participants underwent intradermal injection of 0.1 ml of two units of tuberculin (AJ Vaccines) or saline in the volar aspect of the forearm as previously described *(4, 5, 8)*. At 48 hours clinical induration at the injection site was measured, immediately prior to sampling by 3mm punch biopsy as previously described *(4, 5)*. Additional saline samples from individuals with cured or latent TB, BCG vaccine recipients and healthy volunteers have been described previously *(8)*.

RNA purification from skin biopsy and zebrafish embryo samples

Skin biopsies were homogenized as previously described *(8)*. Pooled zebrafish embryos (25-30 per experimental condition) collected in Qiazol (Qiagen) were homogenized in CK14 lysing kit tubes (Bertin Instruments) using a Precellys Evolution homogenizer (Bertin Instruments) for 10-20 seconds at 5500 rpm. Total RNA from skin biopsies and zebrafish samples was purified using the RNEasy mini and micro kits (Qiagen), respectively, according to the manufacturer's instructions. Genomic DNA was removed using the TURBO DNA-free kit (ThermoFisher).

Transcriptional profiling of skin biopsy and zebrafish larval samples

Genome-wide mRNA sequencing was performed as previously described *(8, 60)*. Complementary DNA (cDNA) libraries were prepared using the KAPA HyperPrep kit (Roche). Sequencing was performed in paired-end mode with the NextSeq 500 High Output 75 Cycle Kit (Illumina) using the NextSeq500 system (Illumina) according to the manufacturer's instructions, generating a median of 22 million (range 12.3-27.9 million) 41 base pair reads per human sample and 16.8 million (range

15.1-18.1 million) reads per zebrafish sample. Transcript alignment and quantitation against the Ensembl GRCh38 human genome assembly release 100 or GRCz11 zebrafish genome assembly release 104 was performed using Kallisto *(61)*. Transcript-level output counts and transcripts per million (TPM) values were summed on gene level and annotated with Ensembl gene ID, gene name, and gene biotype using the R/Bioconductor packages tximport and BiomaRt *(62, 63)*. Downstream analysis was performed using R 3.6.3 on log2 transformed TPM values for protein-coding genes only. TPM values <0.001 were set to 0.001 prior to log2 transformation. To determine the need for and effect of batch correction in the human data, principal component analysis (PCA) was performed using the prcomp R function on the integrated list of 6802 genes with the 10% lowest variance in expression for each library preparation date. This revealed separation of three samples in PC1, likely accounted for by lower RNA concentrations or RIN values compared to the rest of the dataset (Fig. S1A). After batch correction performed using the ComBat function of the sva R package *(64)*, allocating samples with PC1 score <0 and >0 to separate batches, this was no longer evident (Fig. S1B).

Radiographic quantitation of TB severity

Disease severity was evaluated by estimating the extent of radiographic abnormalities and whether cavitation was present on chest x-ray at the time of diagnosis, as previously described *(8, 9)*.

Outlier analysis

The BioBase Bioconductor R package was used to perform outlier analysis based on the z-score outlier detection (ZODET) algorithm *(10)*, to identify transcripts in each TST sample whose expression was significantly higher than the mean expression in control saline samples (>2SD, p value <0.05), with a fold difference filter of >1 log2. Chi-squared tests implemented in R were then used to identify outlier genes statistically enriched in TST samples compared to saline samples, using a p value <0.05. To avoid type 2 error no correction for multiple testing was used in this analysis. In instances where multiple Ensembl gene IDs were associated with a single gene symbol, duplicate gene symbols were removed to retain the replicate with the highest expression for each sample.

Pathway enrichment analysis

The biological pathways represented by the TST transcriptome were identified by Reactome pathway enrichment analysis using XGR as previously described *(65, 66)*. For visualization, 15 pathway groups were identified by hierarchical clustering of Jaccard indices to quantify similarity between the gene compositions of each pathway. For each group the pathway term with the largest number of annotated genes was then selected as representative of enriched biology.

Upstream regulator analysis

TST transcriptome genes whose expression was significantly correlated with radiographic severity of TB disease were identified by Spearman rank correlation, p value <0.05, without correction for multiple testing, to prevent type 2 error. Genes positively and negatively correlated with disease severity were separately subjected to Ingenuity Pathway Analysis (Qiagen) to identify upstream molecules responsible for their transcriptional regulation. This analysis was restricted to molecules annotated with the following functions: cytokine, transmembrane receptor, kinase and transcriptional regulator, representing the canonical components of pathways which mediate transcriptional reprogramming in immune responses. Enriched molecules with an adjusted p value <0.05 were considered statistically significant.

Upstream regulator functional modules

TST gene modules representing the functional activity of their upstream molecule were identified as previously described *(11)*. In brief, we calculated the average correlation coefficient for pairwise correlations of the expression levels of the target genes associated with each predicted upstream regulator. We compared these to the distribution of average correlation coefficients obtained from 100 iterations of randomly selecting equivalent sized groups of genes from the TST transcriptome. Only target gene modules with average correlation coefficients higher than the mean of the distribution of equivalent sized randomly selected groups by ≥2 SD (Z score ≥2) with false discovery rate <0.05, were retained. We visualised these upstream regulator modules as network diagrams

using the Force Atlas two algorithm in Gephi v0.9.2 *(67)*, depicting all statistically over-represented molecules (false discovery rate <0.05) predicted to be upstream of ≥4 target genes.

Transcriptional modules

Interferon inducible transcriptional module gene lists are provided in Table S1. Independently derived human type I and type II interferon inducible gene modules were described previously *(5, 8, 11)*. Two further modules were derived to distinguish type I or type II interferon inducible gene expression using published transcriptional data for primary human keratinocytes stimulated with a selection of cytokines (Gene Expression Omnibus accession: GSE36287) *(68)*. Stimulus-specific modules for type I interferon (interferon alpha) and type II interferon (interferon gamma) were derived by selecting genes overexpressed >4-fold in the cognate cytokine condition relative to all non-cognate conditions combined (paired t test with α of $p<0.05$ without multiple testing correction), excluding genes also induced by each non-cognate cytokine condition, using the same criteria. The babelgene R package (https://igordot.github.io/babelgene/) was used to convert human gene symbols to their respective zebrafish orthologues to generate the zebrafish Stat1 module, excluding zebrafish genes reported to be an orthologue of more than one human gene. The zebrafish type I interferon inducible gene module comprises 360 genes whose expression was significantly induced (≥2 fold, adjusted p value <0.05) six hours after intravenous injection of three day post-fertilisation (dpf) larvae with 1 nl of recombinant interferon phi 1 protein (1 mg/ml) as previously described *(16)*.

Venn diagrams

Area-proportional Venn diagrams visualizing the overlap between constituent genes in transcriptional modules were generated using BioVenn *(69)*.

Zebrafish husbandry

Zebrafish were raised and maintained at 28.5°C following a 14/10 light/dark cycle according to standard protocols *(70)* in University College London (UCL) and Neuro-PSI Zebrafish Facilities. All work was approved by the British Home Office (Project License PP8780756) and the French Ministry for Research and Higher Education (Project Licence 39238). All experiments were performed in accordance with the relevant guidelines and regulations, on larvae up to five days post-fertilisation, before they are protected under the Animals (Scientific Procedures) Act. Adult zebrafish were spawned to collect embryos for experiments. Table S2 lists the lines used in this study *(26, 71, 72)*. Embryos were maintained at 28.5°C in egg water containing 60 µg/ml Tropic Marin Sea Salt (Norwood Aquarium) and anaesthetised with egg water containing 200 µg/ml buffered tricaine (3-aminobenzoic acid ethyl ester) (Sigma-Aldrich) during injection, tail fin transection and imaging. Larvae used for in vivo imaging were maintained in egg water supplemented at 24 hours post-fertilisation (hpf) with 0.003% PTU (1-phenyl-2-thiourea) (Sigma-Aldrich) to inhibit melanisation.

CRISPant Generation

To maximise the likelihood of loss of functional protein we employed a previously described triple-exon targeting approach *(73)*, with the modification that Cas9 protein was not diluted before use. CRISPR RNA (crRNA) (Alt-R CRISPR-Cas9 crRNA), tracrRNA (Alt-R CRISPR-Cas9 tracrRNA) and recombinant Cas9 protein (Alt-R Streptococcus pyogenes Cas9 Nuclease V3) were obtained from Integrated DNA Technologies (IDT). Three pre-designed crRNAs targeting distinct exons were selected for the *stat2* gene, prioritizing those that targeted early, asymmetric (not divisible by three) exons common to both protein-coding transcripts, with low off-target and high on-target scores and in a genomic position which allowed design of primers flanking the target site to generate a ~200 bp amplicon, for verification of mutagenesis by next generation sequencing (MiSeq). crRNA sequences and genomic locations are provided in Table S3. To generate gRNAs equal volumes of crRNA and tracrRNA diluted to 61 µM in Duplex buffer (IDT) were annealed at 95°C for 5 minutes. Equal volumes of gRNA (61 µM) and Cas9 protein (61 µM) were incubated at 37°C for 5 minutes to assemble separate 30.5 µM ribonucleoproteins (RNPs) for each target. Equal volumes of the three RNPs were pooled, prior to injection giving a final concentration of 10.2 µM for each. Negative control "scrambled" crRNAs computationally designed to be non-targeting (Alt-R CRISPRCas9 Negative Control crRNA #1, #2, #3) were prepared and pooled as described above. 0.5 nl of pooled *stat2* RNPs or scrambled RNPs was injected into the yolk sac of single-cell stage wild type or transgenic zebrafish embryos before cell inflation as previously described *(73)*. After injections embryos were

transferred into sterile petri dishes with fresh egg water and maintained at 28.5°C to the appropriate age for experiments, as described below.

Interferon phi 1 stimulation

Three dpf *stat2* CRISPant *Tg(mxa:mCherry)* larvae and scrambled RNP injected siblings were injected in the coelomic cavity with 1 nl of recombinant zebrafish interferon phi 1 protein (1.25 mg/ml), produced as previously described *(74)*. *stat2* and control CRISPants were shuffled so that injections were performed blindly. Bovine serum albumin (BSA) (1.25 mg/ml) was injected as a control. Interferon phi 1 and BSA solutions were supplemented with 0.2% phenol red (Sigma-Aldrich) to visualize the inoculum. Induction of Mxa reporter expression was determined by fluorescence microscopy 24 hours post-injection.

M. marinum infection

M. marinum M strain expressing the pmsp12 mWasabi *(75)* or psMT3 mCherry plasmid *(76)* was cultured using Middlebrook 7H10 agar (Becton Dickinson and Company) supplemented with 0.5% oleic acid/albumin/dextrose/catalase (OADC) (Becton Dickinson and Company), 0.5% glycerol (Sigma-Aldrich) and hygromycin (50 µg/ml) (Fisher Scientific). To generate bacterial suspensions for injection, *M. marinum* from agar plates was cultured statically at 28.5°C for 24-36 hours in 10 ml Middlebrook 7H9 broth (Becton Dickinson and Company) supplemented with 10% albumin/dextrose/catalase (ADC) (Becton Dickinson and Company) and hygromycin (50 µg/ml) (Fisher Scientific). Bacteria were harvested at mid-log growth (optical density (OD)600nm 0.7–1), (OD)600nm 1 representing 10^8 colony forming units (cfu)/ml, washed three times in phosphate buffered saline (PBS) (Gibco) and resuspended in 2% polyvinylpyrrolidone (PVP)40 (Sigma-Aldrich)/PBS containing 10% phenol red (Sigma-Aldrich) to aid visualisation of injections *(77)*.

Zebrafish embryos were manually dechorionated using jeweller's forceps (Dumont #5, World Precision Instruments) prior to bacterial infection. To generate systemic infection, 400 cfu *M. marinum* in a volume of 1 nl were microinjected into the caudal vein of embryos staged at 28-30 hpf. Four days post-infection, embryos were either subjected to fluorescence microscopy to measure disease severity or 25-30 per condition pooled and harvested in Qiazol (Qiagen) for evaluation of immune responses by RNAseq. To generate localised infection, 200 cfu *M. marinum* in a volume of 1 nl were injected into the hindbrain ventricle (HBV) of two dpf zebrafish larvae. Cellular recruitment was evaluated by fluorescence microscopy at 6-18 hours post-infection.

Tailfin transection

Tailfin transections were performed as described previously *(26, 78)*. Briefly, live anaesthetised three dpf zebrafish larvae were transferred with a 1 ml Pasteur pipette (Scientific Laboratory Supplies) to a sterile petri dish containing 2% agarose (Bioline). Transections of the caudal fin were performed using a sterile microscalpel (World Precision Instruments) by applying steady downward pressure to create the incision at the boundary with the notochord. Following injury, larvae were rinsed in egg water, and maintained in individual wells of a 96-well tissue culture plate (TPP) at 28.5°C until live imaging to quantify neutrophil or macrophage recruitment to the site of injury at 1, 6 and 24 hours-post-wound (hpw).

Fluorescence microscopy

All fluorescence microscopy was performed on live, anasethised larvae. For quantitation of bacterial burden and dissemination four days post-infection, steady state neutrophil numbers at two dpf and cellular recruitment at 2-4 dpf, larvae were imaged using an M205FA stereofluorescence microscope (Leica) with a 1x objective. Larvae were imaged on a flat 1% agarose plate for quantitation of severity of mycobacterial infection and steady state neutrophil numbers and a 96-well tissue culture plate (TPP) in which the wells were coated with 1% agarose, for cellular recruitment to tailfin transection. Micro-wells were created in 1% agarose using a Stampwell Larvae 1 device (Idylle) for optimal positioning of 2-3 dpf larvae for imaging of cellular recruitment to hindbrain ventricle *M. marinum* infection. Brightfield and fluorescence images were captured using a DFC365 FX camera (Leica) and exported as 16-bit Tagged Image Format (TIF) files for analysis. For quantitation of steady state macrophage numbers three dpf larvae were imaged in 96-well alignment plates (Funakoshi) containing 75 µl egg water per well using a high-content wide-field fluorescence microscope (Hermes, IDEA Bio-Medical) with a 4x objective, capturing five z planes 50.6 µm apart in four

contiguous fields of view per embryo. We created an ImageJ macro to semi-automate generation of single maximum intensity projection z-stack montages from the Hermes images, which were saved as 16-bit TIF files for analysis (Table S4. Mxa reporter expression was recorded with an EVOS M7000 microscope (ThermoFisher) equipped with a 2x/NA0.06 objective and Texas Red fluorescence cube. Larvae were positioned laterally in micro-wells created in 2% agarose with an in-house-printed stamp. A single fluorescence plane was recorded as the depth of field is sufficient to capture the entire larva. Transmitted light images were also recorded and both were exported as 16-bit TIF files.

Image analysis

To quantify bacterial burden, number of bacterial foci and spatial distribution of bacteria, images were analysed using custom QuantiFish software, previously developed in our group, to enable rapid quantitation of fluorescent foci in zebrafish larvae *(79)*. Mxa reporter fluorescence was measured with ImageJ. Transmitted and fluorescence images were stacked. Images were slightly rotated to horizontality where necessary. A 600x100 pixel rectangular region of interest was defined on the transmitted light image to encompass the entire gut and liver areas. Mean fluorescence intensity was then measured on the fluorescence image. For quantitation of total cell number and recruitment of fluorescent immune cells to the site of tailfin transection we developed a new custom Python script which enables quantitation of integrated fluorescence within concentric zones (known as Sholl circles) *(80)*. To achieve this, the script leverages the OpenCV, NumPy *(81)*, Matplotlib, SciPy (http://www.scipy.org), scikit-image *(82)* and pandas Python libraries to facilitate image processing and data extraction (Table S5. First the user is prompted to select a folder containing images for analysis, as well as the file extensions corresponding to the brightfield and fluorescence images, which are essential for the subsequent steps. The script then iterates through each pair of brightfield and fluorescent images prompting the user to define two points on the brightfield image, which serve as the start and end positions between which to create concentric circular regions *(80)* on the corresponding fluorescence image. The script employs the image processing techniques described in Table S5 to quantify integrated fluorescence of the entire image and that within each region, as a surrogates for the total number of immune cells and the number at each spatial location, respectively and generates output files containing this information. Integrated fluorescence within the first zone (the wound site) and distance from the site of tailfin transection of the zone in which the maximal integrated fluorescence (a surrogate for the highest cell numbers) was detected (identified manually) were used as measures of immune cell recruitment for each zebrafish larva. The number of cells recruited to the site of hindbrain *M. marinum* infection was quantified by manual counting.

Genotyping by next generation sequencing

Genomic DNA extraction

Genomic DNA was extracted from anasethetised individual zebrafish larvae using the modified hot sodium hydroxide and Tris (HotSHOT) method as previously described *(73, 83)*. Briefly, larvae in 96-well plates were incubated in 50 µl base solution (25 mM KOH, 0.2 mM EDTA in water) at 95°C for 30 min then cooled to room temperature, before addition of 50 µl neutralization solution (40 mM Tris-HCL in water).

PCR

Extracted DNA (2 µl per 50 µl reaction) was subjected to PCR using Phusion High-Fidelity DNA Polymerase (New England Biolabs) (98°C for 30 seconds (s), once only, 40 cycles of 98°C for 10 s, 59°C for 30 s, 72°C for 20 s, 72°C for 10 minutes, once only). Sequences and genomic positions of the primers used are provided in Table S3. Successful amplification of a single product of approximately 300 bp was verified by 2% agarose (Bioline) Tris-borate-EDTA (TBE) containing Redsafe (Chembio) gel electrophoresis. PCR products were purified using ExoSAP-IT Express (ThermoFisher), concentration of purified DNA determined by Nanodrop spectrophotometer (ThermoFisher) and samples diluted to 15-25 ng/µl for sequencing.

Next generation sequencing and data analysis

Sequencing was performed by the UCL Fish Genomic Service using the MiSeq Reagent Kit v2 (300-cycles) (Illumina) and the MiSeq system (Illumina) in paired end mode, according to the manufacturer's instructions. Sequencing data were received as two FASTQ files (forward and

reverse) for each sample. Visual sequence analysis was performed using Geneious 10.2.6 (https://www.geneious.com) for initial verification of successful genome editing close to the PAM site. Objective quantitation of the proportion of reads mutated and predicted to be frameshifted was achieved using the ampliCan R package *(84)*, which utilizes the FASTQ files and a metadata file providing the amplicon, protospacer adjacent motif (PAM) and primer sequences (Table S3) and sample information, as previously described *(73)*. AmpliCan was run with default parameters, with the exception that min_freq = 0.005 (mutations at a frequency below this threshold were considered a sequencing error) and average_quality = 25. Mutations present in uninjected or scrambled RNP injected control samples were not included as Cas9 induced mutations.

Statistical analysis

Statistical analysis was performed using GraphPad Prism 9.3.1 for Windows (GraphPad Software) and R3.6.3. Chi-squared tests were used to identify outlier genes statistically enriched in transcriptomic data from TST samples compared to saline samples, with no correction for multiple testing to avoid type 2 error. Spearman rank correlation was used to determine the strength of relationship between TST transcriptome gene expression and TB disease severity (two-tailed), transcript levels of upstream regulator target gene modules and TST random gene modules (one-tailed, positive correlation only) and mean expression of transcriptional modules in TST transcriptomic data with severity of TB disease (two-tailed). The Benjamini-Hochberg correction method for multiple comparisons was used to identify upstream regulator target gene modules with average correlation coefficients significantly higher than the mean of the distribution of equivalent sized randomly selected gene modules by ≥2 SD (Z score ≥2) with false discovery rate <0.05. Survival of *stat2* CRISPant and control zebrafish larvae was compared using a log-rank (Mantel-Cox) test; a p value <0.05 was considered significant. On scatter plots horizontal lines represent median values and error bars indicate the interquartile range. On box and whisker plots horizontal lines represent median values, box limits indicate the interquartile range and whiskers extend between the 5th and 95th percentiles of the data. Two-tailed Mann-Whitney tests were used for two group comparisons of unpaired data; a p value <0.05 was considered significant. Where p values are not presented on graphs, * denotes p<0.05.

REFERENCES AND NOTES

1. A. K. Coussens, S. M. A. Zaidi, B. W. Allwood, P. K. Dewan, G. Gray, M. Kohli, T. Kredo, B. J. Marais, G. B. Marks, L. Martinez, M. Ruhwald, T. J. Scriba, J. A. Seddon, P. Tisile, D. F. Warner, R. J. Wilkinson, H. Esmail, R. M. G. J. Houben, International Consensus for Early TB (ICE-TB) group, Classification of early tuberculosis states to guide research for improved care and prevention: an international Delphi consensus exercise. *Lancet Respir. Med.* **12**, 484–498 (2024).

2. A. M. Cadena, S. M. Fortune, J. L. Flynn, Heterogeneity in tuberculosis. *Nat. Rev. Immunol.* **17**, 691–702 (2017).

3. S. H. E. Kaufmann, C. Lange, M. Rao, K. N. Balaji, M. Lotze, M. Schito, A. I. Zumla, M. Maeurer, Progress in tuberculosis vaccine development and host-directed therapies--a state of the art review. *Lancet Respir. Med.* **2**, 301–320 (2014).

4. G. S. Tomlinson, T. J. Cashmore, P. T. G. Elkington, J. Yates, R. J. Lehloenya, J. Tsang, M. Brown, R. F. Miller, K. Dheda, D. R. Katz, B. M. Chain, M. Noursadeghi, Transcriptional profiling of innate and adaptive human immune responses to mycobacteria in the tuberculin skin test. *Eur. J. Immunol.* **41**, 3253–3260 (2011).

5. L. C. K. Bell, G. Pollara, M. Pascoe, G. S. Tomlinson, R. J. Lehloenya, J. Roe, R. Meldau, R. F. Miller, A. Ramsay, B. M. Chain, K. Dheda, M. Noursadeghi, In Vivo Molecular Dissection of the Effects of HIV-1 in Active Tuberculosis. *PLoS Pathog.* **12**, e1005469 (2016).

6. M.-J. Kim, H. C. Wainwright, M. Locketz, L.-G. Bekker, G. B. Walther, C. Dittrich, A. Visser, W. Wang, F.-F. Hsu, U. Wiehart, L. Tsenova, G. Kaplan, D. G. Russell, Caseation of human tuberculosis granulomas correlates with elevated host lipid metabolism. *EMBO Mol. Med.* **2**, 258–274 (2010).

7. L. Ramakrishnan, The zebrafish guide to tuberculosis immunity and treatment. *Cold Spring Harb.*

Symp. Quant. Biol. **78**, 179–192 (2013).

8. G. Pollara, C. T. Turner, J. Rosenheim, A. Chandran, L. C. K. Bell, A. Khan, A. Patel, L. F. Peralta, A. Folino, A. Akarca, C. Venturini, T. Baker, S. Ecker, F. L. M. Ricciardolo, T. Marafioti, C. Ugarte-Gil, D. A. J. Moore, B. M. Chain, G. S. Tomlinson, M. Noursadeghi, Exaggerated IL-17A activity in human in vivo recall responses discriminates active tuberculosis from latent infection and cured disease. *Sci. Transl. Med.* **13**, eabg7673 (2021).

9. A. P. Ralph, M. Ardian, A. Wiguna, G. P. Maguire, N. G. Becker, G. Drogumuller, M. J. Wilks, G. Waramori, E. Tjitra, null Sandjaja, E. Kenagalem, G. J. Pontororing, N. M. Anstey, P. M. Kelly, A simple, valid, numerical score for grading chest x-ray severity in adult smear-positive pulmonary tuberculosis. *Thorax* **65**, 863–869 (2010).

10. D. L. Roden, G. W. Sewell, A. Lobley, A. P. Levine, A. M. Smith, A. W. Segal, ZODET: software for the identification, analysis and visualisation of outlier genes in microarray expression data. *PloS One* **9**, e81123 (2014).

11. A. Chandran, J. Rosenheim, G. Nageswaran, L. Swadling, G. Pollara, R. K. Gupta, A. R. Burton, J. A. Guerra-Assunção, A. Woolston, T. Ronel, C. Pade, J. M. Gibbons, B. Sanz-Magallon Duque De Estrada, M. Robert de Massy, M. Whelan, A. Semper, T. Brooks, D. M. Altmann, R. J. Boyton, Á. McKnight, G. Captur, C. Manisty, T. A. Treibel, J. C. Moon, G. S. Tomlinson, M. K. Maini, B. M. Chain, M. Noursadeghi, COVIDsortium Investigators, Rapid synchronous type 1 IFN and virus-specific T cell responses characterize first wave non-severe SARS-CoV-2 infections. *Cell Rep. Med.* **3**, 100557 (2022).

12. R. L. Kinsella, D. X. Zhu, G. A. Harrison, A. E. Mayer Bridwell, J. Prusa, S. M. Chavez, C. L. Stallings, Perspectives and Advances in the Understanding of Tuberculosis. *Annu. Rev. Pathol. Mech. Dis.* **16**, 377–408 (2021).

13. F. Paduano, E. Gaudio, A. A. Mensah, S. Pinton, F. Bertoni, F. Trapasso, T-Cell Leukemia/Lymphoma 1 (TCL1): An Oncogene Regulating Multiple Signaling Pathways. *Front. Oncol.* **8**, 317 (2018).

14. F. McNab, K. Mayer-Barber, A. Sher, A. Wack, A. O'Garra, Type I interferons in infectious disease. *Nat. Rev. Immunol.* **15**, 87–103 (2015).

15. C. Langevin, E. Aleksejeva, G. Passoni, N. Palha, J.-P. Levraud, P. Boudinot, The antiviral innate immune response in fish: evolution and conservation of the IFN system. *J. Mol. Biol.* **425**, 4904–4920 (2013).

16. J.-P. Levraud, L. Jouneau, V. Briolat, V. Laghi, P. Boudinot, IFN-Stimulated Genes in Zebrafish and Humans Define an Ancient Arsenal of Antiviral Immunity. *J. Immunol. Baltim. Md 1950* **203**, 3361–3373 (2019).

17. K. Blaszczyk, H. Nowicka, K. Kostyrko, A. Antonczyk, J. Wesoly, H. A. R. Bluyssen, The unique role of STAT2 in constitutive and IFN-induced transcription and antiviral responses. *Cytokine Growth Factor Rev.* **29**, 71–81 (2016).

18. A. Begitt, M. Droescher, T. Meyer, C. D. Schmid, M. Baker, F. Antunes, K.-P. Knobeloch, M. R. Owen, R. Naumann, T. Decker, U. Vinkemeier, STAT1-cooperative DNA binding distinguishes type 1 from type 2 interferon signaling. *Nat. Immunol.* **15**, 168–176 (2014).

19. J. W. Schoggins, Interferon-Stimulated Genes: What Do They All Do? *Annu. Rev. Virol.* **6**, 567–584 (2019).

20. H. Clay, J. M. Davis, D. Beery, A. Huttenlocher, S. E. Lyons, L. Ramakrishnan, Dichotomous role of the macrophage in early Mycobacterium marinum infection of the zebrafish. *Cell Host Microbe* **2**, 29–39 (2007).

612 21. A. J. Pagán, C.-T. Yang, J. Cameron, L. E. Swaim, F. Ellett, G. J. Lieschke, L. Ramakrishnan,
613 Myeloid Growth Factors Promote Resistance to Mycobacterial Infection by Curtailing Granuloma
614 Necrosis through Macrophage Replenishment. *Cell Host Microbe* **18**, 15–26 (2015).

615 22. R. D. Berg, S. Levitte, M. P. O'Sullivan, S. M. O'Leary, C. J. Cambier, J. Cameron, K. K. Takaki,
616 C. B. Moens, D. M. Tobin, J. Keane, L. Ramakrishnan, Lysosomal Disorders Drive Susceptibility to
617 Tuberculosis by Compromising Macrophage Migration. *Cell* **165**, 139–152 (2016).

618 23. C.-T. Yang, C. J. Cambier, J. M. Davis, C. J. Hall, P. S. Crosier, L. Ramakrishnan, Neutrophils
619 exert protection in the early tuberculous granuloma by oxidative killing of mycobacteria
620 phagocytosed from infected macrophages. *Cell Host Microbe* **12**, 301–312 (2012).

621 24. P. M. Elks, S. Brizee, M. van der Vaart, S. R. Walmsley, F. J. van Eeden, S. A. Renshaw, A. H.
622 Meijer, Hypoxia inducible factor signaling modulates susceptibility to mycobacterial infection via a
623 nitric oxide dependent mechanism. *PLoS Pathog.* **9**, e1003789 (2013).

624 25. I. Rauch, M. Müller, T. Decker, The regulation of inflammation by interferons and their STATs.
625 *JAK-STAT* **2**, e23820 (2013).

626 26. S. A. Renshaw, C. A. Loynes, D. M. I. Trushell, S. Elworthy, P. W. Ingham, M. K. B. Whyte, A
627 transgenic zebrafish model of neutrophilic inflammation. *Blood* **108**, 3976–3978 (2006).

628 27. C. Gray, C. A. Loynes, M. K. B. Whyte, D. C. Crossman, S. A. Renshaw, T. J. A. Chico,
629 Simultaneous intravital imaging of macrophage and neutrophil behaviour during inflammation using
630 a novel transgenic zebrafish. *Thromb. Haemost.* **105**, 811–819 (2011).

631 28. F. Ellett, L. Pase, J. W. Hayman, A. Andrianopoulos, G. J. Lieschke, mpeg1 promoter transgenes
632 direct macrophage-lineage expression in zebrafish. *Blood* **117**, e49-56 (2011).

633 29. M. P. R. Berry, C. M. Graham, F. W. McNab, Z. Xu, S. A. A. Bloch, T. Oni, K. A. Wilkinson, R.
634 Banchereau, J. Skinner, R. J. Wilkinson, C. Quinn, D. Blankenship, R. Dhawan, J. J. Cush, A. Mejias,
635 O. Ramilo, O. M. Kon, V. Pascual, J. Banchereau, D. Chaussabel, A. O'Garra, An interferon-
636 inducible neutrophil-driven blood transcriptional signature in human tuberculosis. *Nature* **466**, 973–
637 977 (2010).

638 30. C. I. Bloom, C. M. Graham, M. P. R. Berry, K. A. Wilkinson, T. Oni, F. Rozakeas, Z. Xu, J.
639 Rossello-Urgell, D. Chaussabel, J. Banchereau, V. Pascual, M. Lipman, R. J. Wilkinson, A. O'Garra,
640 Detectable Changes in The Blood Transcriptome Are Present after Two Weeks of Antituberculosis
641 Therapy. *PLOS ONE* **7**, e46191 (2012).

642 31. T. H. M. Ottenhoff, R. H. Dass, N. Yang, M. M. Zhang, H. E. E. Wong, E. Sahiratmadja, C. C.
643 Khor, B. Alisjahbana, R. van Crevel, S. Marzuki, M. Seielstad, E. van de Vosse, M. L. Hibberd,
644 Genome-Wide Expression Profiling Identifies Type 1 Interferon Response Pathways in Active
645 Tuberculosis. *PLOS ONE* **7**, e45839 (2012).

646 32. K. D. Mayer-Barber, B. B. Andrade, D. L. Barber, S. Hieny, C. G. Feng, P. Caspar, S. Oland, S.
647 Gordon, A. Sher, Innate and Adaptive Interferons Suppress IL-1α and IL-1β Production by Distinct
648 Pulmonary Myeloid Subsets during Mycobacterium tuberculosis Infection. *Immunity* **35**, 1023–1034
649 (2011).

650 33. K. D. Mayer-Barber, B. B. Andrade, S. D. Oland, E. P. Amaral, D. L. Barber, J. Gonzales, S. C.
651 Derrick, R. Shi, N. P. Kumar, W. Wei, X. Yuan, G. Zhang, Y. Cai, S. Babu, M. Catalfamo, A. M.
652 Salazar, L. E. Via, C. E. Barry, A. Sher, Host-directed therapy of tuberculosis based on interleukin-
653 1 and type I interferon crosstalk. *Nature* **511**, 99–103 (2014).

654 34. D. X. Ji, L. H. Yamashiro, K. J. Chen, N. Mukaida, I. Kramnik, K. H. Darwin, R. E. Vance, Type I
655 interferon-driven susceptibility to Mycobacterium tuberculosis is mediated by IL-1Ra. *Nat. Microbiol.*
656 **4**, 2128–2135 (2019).

35. D. I. Kotov, O. V. Lee, S. A. Fattinger, C. A. Langner, J. V. Guillen, J. M. Peters, A. Moon, E. M. Burd, K. C. Witt, D. B. Stetson, D. L. Jaye, B. D. Bryson, R. E. Vance, Early cellular mechanisms of type I interferon-driven susceptibility to tuberculosis. *Cell* **186**, 5536-5553.e22 (2023).

36. L. Moreira-Teixeira, K. Mayer-Barber, A. Sher, A. O'Garra, Type I interferons in tuberculosis: Foe and occasionally friend. *J. Exp. Med.* **215**, 1273–1285 (2018).

37. I. Kramnik, G. Beamer, Mouse models of human TB pathology: roles in the analysis of necrosis and the development of host-directed therapies. *Semin. Immunopathol.* **38**, 221–237 (2016).

38. S. Giosué, M. Casarini, L. Alemanno, G. Galluccio, P. Mattia, G. Pedicelli, L. Rebek, A. Bisetti, F. Ameglio, Effects of aerosolized interferon-alpha in patients with pulmonary tuberculosis. *Am. J. Respir. Crit. Care Med.* **158**, 1156–1162 (1998).

39. P. Zarogoulidis, I. Kioumis, N. Papanas, K. Manika, T. Kontakiotis, A. Papagianis, K. Zarogoulidis, The effect of combination IFN-alpha-2a with usual antituberculosis chemotherapy in non-responding tuberculosis and diabetes mellitus: a case report and review of the literature. *J. Chemother.* **24**, 173–177 (2012).

40. D. Mansoori, S. Tavana, M. Mirsaeidi, M. Yazdanpanah, H. Sohrabpour, The Efficacy of Interferon-α in the Treatment of Multidrug Resistant Tuberculosis. *TANAFFOS* **1**, 29–34 (2002).

41. Y. E. Liu, P. A. Darrah, J. J. Zeppa, M. Kamath, F. Laboune, D. C. Douek, P. Maiello, M. Roederer, J. L. Flynn, R. A. Seder, P. Khatri, Blood transcriptional correlates of BCG-induced protection against tuberculosis in rhesus macaques. *Cell Rep. Med.* **4**, 101096 (2023).

42. L. B. Tezera, M. K. Bielecka, A. Chancellor, M. T. Reichmann, B. A. Shammari, P. Brace, A. Batty, A. Tocheva, S. Jogai, B. G. Marshall, M. Tebruegge, S. N. Jayasinghe, S. Mansour, P. T. Elkington, B. Aldridge, Ed. Dissection of the host-pathogen interaction in human tuberculosis using a bioengineered 3-dimensional model. *eLife* **6**, e21283 (2017).

43. V. Torraca, C. Cui, R. Boland, J.-P. Bebelman, A. M. van der Sar, M. J. Smit, M. Siderius, H. P. Spaink, A. H. Meijer, The CXCR3-CXCL11 signaling axis mediates macrophage recruitment and dissemination of mycobacterial infection. *Dis. Model. Mech.* **8**, 253–269 (2015).

44. J. M. Davis, H. Clay, J. L. Lewis, N. Ghori, P. Herbomel, L. Ramakrishnan, Real-time visualization of mycobacterium-macrophage interactions leading to initiation of granuloma formation in zebrafish embryos. *Immunity* **17**, 693–702 (2002).

45. D. M. Tobin, F. J. Roca, S. F. Oh, R. McFarland, T. W. Vickery, J. P. Ray, D. C. Ko, Y. Zou, N. D. Bang, T. T. H. Chau, J. C. Vary, T. R. Hawn, S. J. Dunstan, J. J. Farrar, G. E. Thwaites, M.-C. King, C. N. Serhan, L. Ramakrishnan, Host genotype-specific therapies can optimize the inflammatory response to mycobacterial infections. *Cell* **148**, 434–446 (2012).

46. A.-L. Neehus, B. Carey, M. Landekic, P. Panikulam, G. Deutsch, M. Ogishi, C. A. Arango-Franco, Q. Philippot, M. Modaresi, I. Mohammadzadeh, M. Corcini Berndt, D. Rinchai, T. Le Voyer, J. Rosain, M. Momenilandi, M. Martin-Fernandez, T. Khan, J. Bohlen, J. E. Han, A. Deslys, M. Bernard, T. Gajardo-Carrasco, C. Soudée, C. Le Floc'h, M. Migaud, Y. Seeleuthner, M.-S. Jang, E. Nikolouli, S. Seyedpour, H. Begueret, J.-F. Emile, P. Le Guen, G. Tavazzi, C. N. J. Colombo, F. C. Marzani, M. Angelini, F. Trespidi, S. Ghirardello, N. Alipour, A. Molitor, R. Carapito, M. Mazloomrezaei, H. Rokni-Zadeh, M. Changi-Ashtiani, C. Brouzes, P. Vargas, A. Borghesi, N. Lachmann, S. Bahram, B. Crestani, S. Pahari, L. S. Schlesinger, N. Marr, D. Bugonovic, S. Boisson-Dupuis, V. Béziat, L. Abel, R. Borie, L. R. Young, R. Deterding, M. Shahrooei, N. Rezaei, N. Parvaneh, D. Craven, P. Gros, D. Malo, F. E. Sepulveda, L. M. Nogee, N. Aladjidi, B. C. Trapnell, J.-L. Casanova, J. Bustamante, Human inherited CCR2 deficiency underlies progressive polycystic lung disease. *Cell* **187**, 390-408.e23 (2024).

47. K. B. Walters, J. M. Green, J. C. Surfus, S. K. Yoo, A. Huttenlocher, Live imaging of neutrophil

703 motility in a zebrafish model of WHIM syndrome. *Blood* **116**, 2803–2811 (2010).

704 48. M. H. Lehmann, L. E. Torres-Domínguez, P. J. R. Price, C. Brandmüller, C. J. Kirschning, G.
705 Sutter, CCL2 expression is mediated by type I IFN receptor and recruits NK and T cells to the lung
706 during MVA infection. *J. Leukoc. Biol.* **99**, 1057–1064 (2016).

707 49. M. Buttmann, C. Merzyn, P. Rieckmann, Interferon-beta induces transient systemic IP-
708 10/CXCL10 chemokine release in patients with multiple sclerosis. *J. Neuroimmunol.* **156**, 195–203
709 (2004).

710 50. C. J. Cambier, K. K. Takaki, R. P. Larson, R. E. Hernandez, D. M. Tobin, K. B. Urdahl, C. L.
711 Cosma, L. Ramakrishnan, Mycobacteria manipulate macrophage recruitment through coordinated
712 use of membrane lipids. *Nature* **505**, 218–222 (2014).

713 51. L. Abel, J. Fellay, D. W. Haas, E. Schurr, G. Srikrishna, M. Urbanowski, N. Chaturvedi, S.
714 Srinivasan, D. H. Johnson, W. R. Bishai, Genetics of human susceptibility to active and latent
715 tuberculosis: present knowledge and future perspectives. *Lancet Infect. Dis.* **18**, e64–e75 (2018).

716 52. A. Khadela, V. P. Chavda, H. Postwala, Y. Shah, P. Mistry, V. Apostolopoulos, Epigenetics in
717 Tuberculosis: Immunomodulation of Host Immune Response. *Vaccines* **10**, 1740 (2022).

718 53. A. L. Jacobs, Infective dose in pulmonary tuberculosis. *Tubercle* **22**, 266–271 (1941).

719 54. C. R. Plumlee, F. J. Duffy, B. H. Gern, J. L. Delahaye, S. B. Cohen, C. R. Stoltzfus, T. R. Rustad,
720 S. G. Hansen, M. K. Axthelm, L. J. Picker, J. D. Aitchison, D. R. Sherman, V. V. Ganusov, M. Y.
721 Gerner, D. E. Zak, K. B. Urdahl, Ultra-low Dose Aerosol Infection of Mice with Mycobacterium
722 tuberculosis More Closely Models Human Tuberculosis. *Cell Host Microbe* **29**, 68-82.e5 (2021).

723 55. J.-L. Casanova, M. S. Anderson, Unlocking life-threatening COVID-19 through two types of
724 inborn errors of type I IFNs. *J. Clin. Invest.* **133**, e166283.

725 56. P. Elkington, T. Shiomi, R. Breen, R. K. Nuttall, C. A. Ugarte-Gil, N. F. Walker, L. Saraiva, B.
726 Pedersen, F. Mauri, M. Lipman, D. R. Edwards, B. D. Robertson, J. D'Armiento, J. S. Friedland,
727 MMP-1 drives immunopathology in human tuberculosis and transgenic mice. *J. Clin. Invest.* **121**,
728 1827–1833 (2011).

729 57. L. Guglielmetti, A. Cazzadori, M. Conti, F. Boccafoglio, A. Vella, R. Ortolani, E. Concia,
730 Lymphocyte subpopulations in active tuberculosis: association with disease severity and the QFT-
731 GIT assay. *Int. J. Tuberc. Lung Dis. Off. J. Int. Union Tuberc. Lung Dis.* **17**, 825–828 (2013).

732 58. J. O. Jurado, V. Pasquinelli, I. B. Alvarez, D. Peña, A. I. Rovetta, N. L. Tateosian, H. E. Romeo,
733 R. M. Musella, D. Palmero, H. E. Chuluyán, V. E. García, IL-17 and IFN-γ expression in lymphocytes
734 from patients with active tuberculosis correlates with the severity of the disease. *J. Leukoc. Biol.* **91**,
735 991–1002 (2012).

736 59. Z. Hasan, B. Jamil, J. Khan, R. Ali, M. A. Khan, N. Nasir, M. S. Yusuf, S. Jamil, M. Irfan, R.
737 Hussain, Relationship between circulating levels of IFN-gamma, IL-10, CXCL9 and CCL2 in
738 pulmonary and extrapulmonary tuberculosis is dependent on disease severity. *Scand. J. Immunol.*
739 **69**, 259–267 (2009).

740 60. J. Roe, C. Venturini, R. K. Gupta, C. Gurry, B. M. Chain, Y. Sun, J. Southern, C. Jackson, M. C.
741 Lipman, R. F. Miller, A. R. Martineau, I. Abubakar, M. Noursadeghi, Blood Transcriptomic
742 Stratification of Short-term Risk in Contacts of Tuberculosis. *Clin. Infect. Dis. Off. Publ. Infect. Dis.*
743 *Soc. Am.* **70**, 731–737 (2020).

744 61. N. L. Bray, H. Pimentel, P. Melsted, L. Pachter, Near-optimal probabilistic RNA-seq
745 quantification. *Nat. Biotechnol.* **34**, 525–527 (2016).

746 62. C. Soneson, M. I. Love, M. D. Robinson, Differential analyses for RNA-seq: transcript-level
747 estimates improve gene-level inferences. *F1000Research* **4**, 1521 (2015).

748 63. S. Durinck, P. T. Spellman, E. Birney, W. Huber, Mapping identifiers for the integration of
749 genomic datasets with the R/Bioconductor package biomaRt. *Nat. Protoc.* **4**, 1184–1191 (2009).

750 64. J. T. Leek, W. E. Johnson, H. S. Parker, A. E. Jaffe, J. D. Storey, The sva package for removing
751 batch effects and other unwanted variation in high-throughput experiments. *Bioinforma. Oxf. Engl.*
752 **28**, 882–883 (2012).

753 65. H. Fang, B. Knezevic, K. L. Burnham, J. C. Knight, XGR software for enhanced interpretation of
754 genomic summary data, illustrated by application to immunological traits. *Genome Med.* **8**, 129
755 (2016).

756 66. C. T. Turner, J. Brown, E. Shaw, I. Uddin, E. Tsaliki, J. K. Roe, G. Pollara, Y. Sun, J. M. Heather,
757 M. Lipman, B. Chain, M. Noursadeghi, Persistent T Cell Repertoire Perturbation and T Cell
758 Activation in HIV After Long Term Treatment. *Front. Immunol.* **12**, 634489 (2021).

759 67. M. Jacomy, T. Venturini, S. Heymann, M. Bastian, ForceAtlas2, a continuous graph layout
760 algorithm for handy network visualization designed for the Gephi software. *PloS One* **9**, e98679
761 (2014).

762 68. W. R. Swindell, X. Xing, P. E. Stuart, C. S. Chen, A. Aphale, R. P. Nair, J. J. Voorhees, J. T.
763 Elder, A. Johnston, J. E. Gudjonsson, Heterogeneity of inflammatory and cytokine networks in
764 chronic plaque psoriasis. *PloS One* **7**, e34594 (2012).

765 69. T. Hulsen, J. de Vlieg, W. Alkema, BioVenn - a web application for the comparison and
766 visualization of biological lists using area-proportional Venn diagrams. *BMC Genomics* **9**, 488 (2008).

767 70. C. Nusslein-Volhard, *Zebrafish: A Practical Approach* R. Dahm, Ed. (Oxford University Press,
768 Oxford, 1 edition., 2002).

769 71. G. Maarifi, N. Smith, S. Maillet, O. Moncorgé, C. Chamontin, J. Edouard, F. Sohm, F. P. Blanchet,
770 J.-P. Herbeuval, G. Lutfalla, J.-P. Levraud, N. J. Arhel, S. Nisole, TRIM8 is required for virus-induced
771 IFN response in human plasmacytoid dendritic cells. *Sci. Adv.* **5**, eaax3511 (2019).

772 72. K. Voelz, R. L. Gratacap, R. T. Wheeler, A zebrafish larval model reveals early tissue-specific
773 innate immune responses to Mucor circinelloides. *Dis. Model. Mech.* **8**, 1375–1388 (2015).

774 73. F. Kroll, G. T. Powell, M. Ghosh, G. Gestri, P. Antinucci, T. J. Hearn, H. Tunbak, S. Lim, H. W.
775 Dennis, J. M. Fernandez, D. Whitmore, E. Dreosti, S. W. Wilson, E. J. Hoffman, J. Rihel, S. C. Ekker,
776 D. Y. Stainier, D. Balciunas, Eds. A simple and effective F0 knockout method for rapid screening of
777 behaviour and other complex phenotypes. *eLife* **10**, e59683 (2021).

778 74. D. Aggad, M. Mazel, P. Boudinot, K. E. Mogensen, O. J. Hamming, R. Hartmann, S. Kotenko,
779 P. Herbomel, G. Lutfalla, J.-P. Levraud, The two groups of zebrafish virus-induced interferons signal
780 via distinct receptors with specific and shared chains. *J. Immunol. Baltim. Md 1950* **183**, 3924–3931
781 (2009).

782 75. K. Takaki, J. M. Davis, K. Winglee, L. Ramakrishnan, Evaluation of the pathogenesis and
783 treatment of Mycobacterium marinum infection in zebrafish. *Nat. Protoc.* **8**, 1114–1124 (2013).

784 76. L. M. van Leeuwen, M. van der Kuip, S. A. Youssef, A. de Bruin, W. Bitter, A. M. van Furth, A.
785 M. van der Sar, Modeling tuberculous meningitis in zebrafish using Mycobacterium marinum. *Dis.*
786 *Model. Mech.* **7**, 1111–1122 (2014).

787 77. E. L. Benard, A. M. van der Sar, F. Ellett, G. J. Lieschke, H. P. Spaink, A. H. Meijer, Infection of
788 zebrafish embryos with intracellular bacterial pathogens. *J. Vis. Exp. JoVE* (2012),

doi:10.3791/3781.

78. R. N. Wilkinson, S. Elworthy, P. W. Ingham, F. J. M. van Eeden, A method for high-throughput PCR-based genotyping of larval zebrafish tail biopsies. *BioTechniques* **55**, 314–316 (2013).

79. D. R. Stirling, O. Suleyman, E. Gil, P. M. Elks, V. Torraca, M. Noursadeghi, G. S. Tomlinson, Analysis tools to quantify dissemination of pathology in zebrafish larvae. *Sci. Rep.* **10**, 3149 (2020).

80. D. A. Sholl, Dendritic organization in the neurons of the visual and motor cortices of the cat. *J. Anat.* **87**, 387–406 (1953).

81. S. van der Walt, S. C. Colbert, G. Varoquaux, The NumPy Array: A Structure for Efficient Numerical Computation. *Comput. Sci. Eng.* **13**, 22–30 (2011).

82. S. van der Walt, J. L. Schönberger, J. Nunez-Iglesias, F. Boulogne, J. D. Warner, N. Yager, E. Gouillart, T. Yu, scikit-image contributors, scikit-image: image processing in Python. *PeerJ* **2**, e453 (2014).

83. N. D. Meeker, S. A. Hutchinson, L. Ho, N. S. Trede, Method for isolation of PCR-ready genomic DNA from zebrafish tissues. *BioTechniques* **43**, 610, 612, 614 (2007).

84. K. Labun, X. Guo, A. Chavez, G. Church, J. A. Gagnon, E. Valen, Accurate analysis of genuine CRISPR editing events with ampliCan. *Genome Res.* **29**, 843–847 (2019).

ACKNOWLEDGEMENTS

We thank Michelle Berin and Victoria Dean (Clinical Research Nurses, UCL Division of Infection and Immunity) and Mylah Ramirez (Research Nurse, Barts Health NHS Trust) for support with research governance, participant recruitment and sample collection. We thank the UCL Zebrafish Facility staff, particularly Heather Callaway, Jenna Hakkesteeg, Karen Dunford, Carole Wilson and Elise Hitchcock for maintenance of the zebrafish lines used in this study, especially during the first wave of the COVID-19 pandemic. We thank UCL Genomics for library preparation and sequencing of samples for transcriptional profiling (www.ucl.ac.uk/child-health/research/genetics-and-genomic-medicine/ucl-genomics). We thank Alex Lubin and Katie-Jo Miller for next generation sequencing of zebrafish samples for genotyping. This work has benefited from the facilities and expertise of CELPHEDIA-TEFOR, UAR2010 TEFOR Paris-Saclay (TEFOR Infrastructure - Investissement d'avenir - ANR-II-INBS-0014) and from the Recombinant Protein Platform of the Institut Pasteur, Paris.

FUNDING

UK Medical Research Council Clinician Scientist Fellowship MR/N007727/1 (GST)

Wellcome Trust Investigator Award 207511/Z/17/Z (MN)

Sir Henry Dale Fellowship jointly funded by the Wellcome Trust and the Royal Society 105570/Z/14/Z (PME)

Fondation pour la Recherche Medicale grant EQU202203014646 (J-PL)

National Institute of Health Research Biomedical Research Centre Funding to University College Hospitals NHS Foundation Trust and University College London (GST, MN)

This research was funded in whole, or in part, by the Wellcome Trust [207511/Z/17/Z, 105570/Z/14/Z]. For the purpose of Open Access, the author has applied a CC BY public copyright licence to any Author Accepted Manuscript version arising from this submission.

AUTHOR CONTRIBUTIONS

Conceived the study: GST, MN

Collected the data: ASS, BSMDDE, JR, ET, GP, J-PL, GST

Provided resources or analysis tools: ASS, BSMDDE, JR, CTT, MCIL, HK, GP, PME, EMP, J-PL, MN, GST

Performed the data analysis / interpretation: ASS, BSMDDE, JR, CTT, GP, PME, EMP, J-PL, MN, GST

Prepared the manuscript draft: GST, ASS, BSMDDE

All authors reviewed and contributed to the final manuscript.

COMPETING INTERESTS

The authors declare that they have no competing interests.

DATA AND MATERIALS AVAILABILITY

Human RNAseq data are already available in the ArrayExpress repository under accession number E-MTAB-6816. Zebrafish RNAseq data will be made available in ArrayExpress at the time of peer reviewed publication of the manuscript. The source code and manual for QuantiFish software used for analysis of bacterial burden and dissemination in zebrafish larvae are available at https://github.com/DavidStirling/QuantiFish. The ImageJ macro used to generate montages from the Hermes images and source code and manual for the Python script used for analysis of steady state cell numbers and cellular recruitment in zebrafish are available at https://github.com/AndSzyShe/particle_analysis. Source data for figure panels with fewer than 20 data points are available in Data file S1.

FIGURES

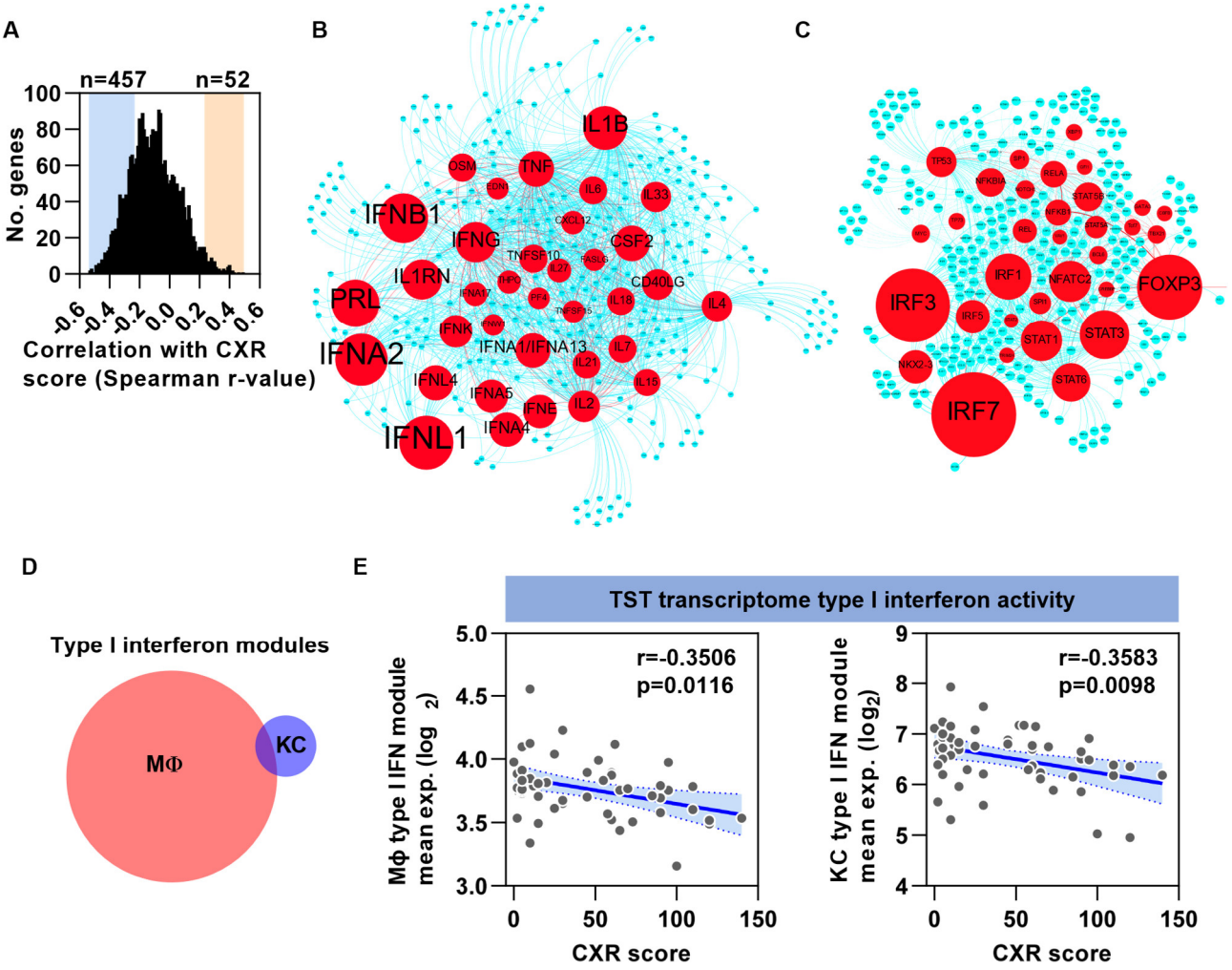

Fig. 1. Reduced type I interferon activity in the TST transcriptome is associated with increased severity of human TB disease. (A) Frequency distribution of the correlation coefficients for the relationship between the abundance of each of the 3222 transcripts within the tuberculin skin test (TST) transcriptome derived from 51 individuals with pulmonary tuberculosis (TB) and radiographic disease severity. Coloured boxes highlight statistically significant correlations ($p<0.05$). **(B, C)** Network diagrams of statistically significant (FDR<0.05) cytokines **(B)** and transcription factors **(C)** predicted to be upstream regulators (red) of target gene modules (blue) whose expression is negatively correlated with radiological TB severity. Size of the nodes for upstream regulators is proportional to -Log10 p value. Nodes were clustered using the Force Atlas 2 algorithm in Gephi (version 0.9.2). **(D, E)** The inverse relationship between average expression in each TST sample of two distinct, independently derived gene modules representing type I interferon activity **(D)** with TB severity **(E)**. r values and p values were derived from two-tailed Spearman rank correlations. CXR = Chest x-ray, MΦ = Macrophage, KC = Keratinocyte.

869

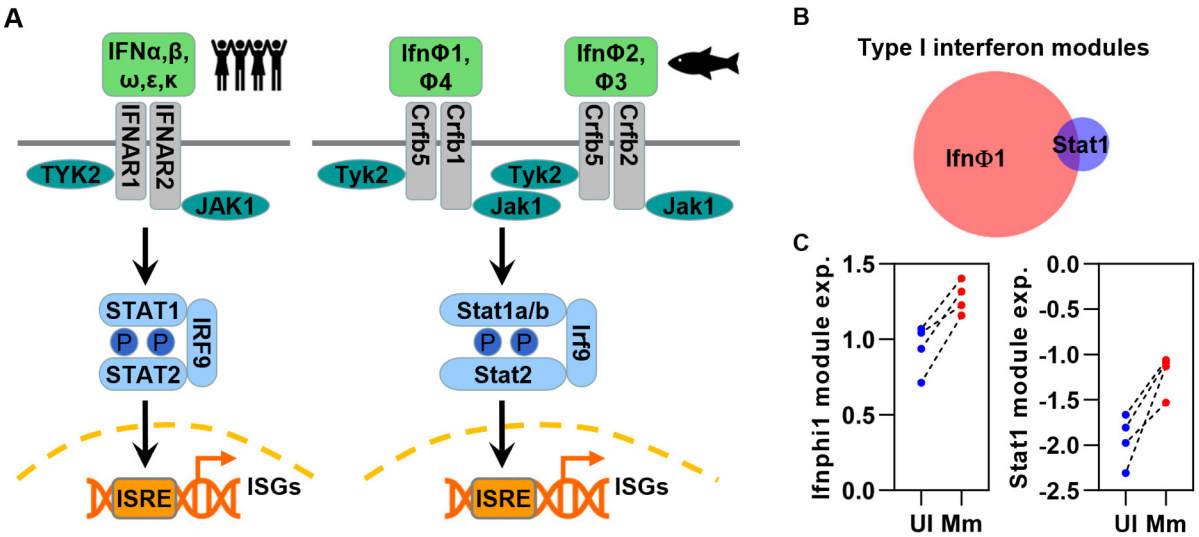

870

871 **Fig. 2. *M. marinum* infection induces a type I interferon response in zebrafish larvae.**
872 **(A)** Schematic representation of the human canonical type I interferon signalling pathway (left) which
873 is highly conserved in zebrafish (right). **(B, C)** The average expression of two largely non-overlapping
874 **(B)** type I interferon inducible gene modules derived from independent data (Table S1) is elevated
875 in *M. marinum* (Mm) infected embryos (4 days post-intravenous infection) compared with uninfected
876 (UI) siblings **(C)**. Data are from four independent experiments.

877

878

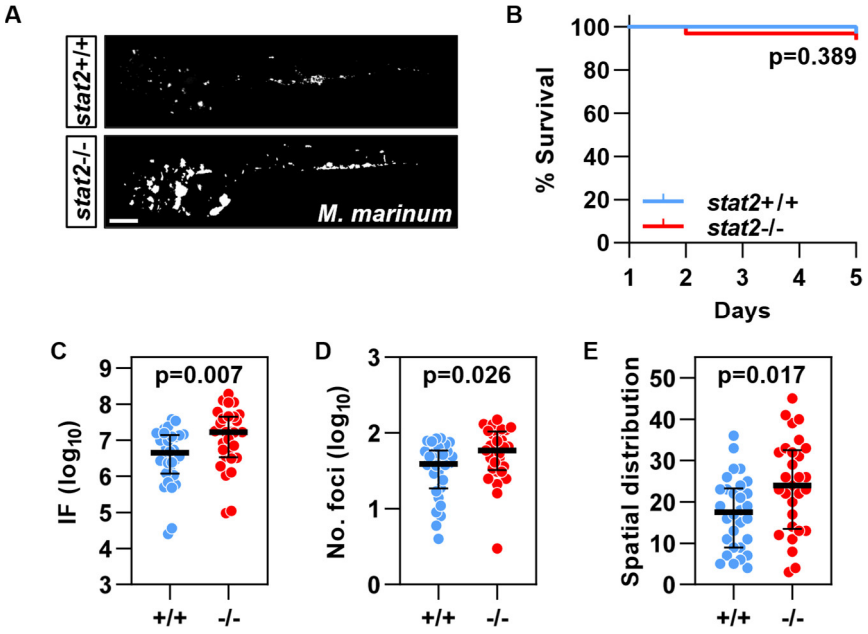

Fig. 3. Increased severity of *M. marinum* infection in *stat2* CRISPants. (A) *stat2* CRISPant (*stat2*-/-) and control ribonucleoprotein (RNP) injected (*stat2*+/+) zebrafish larvae four days post intravenous infection with 400 colony forming units (cfu) mCherry-expressing *M. marinum*. Scale bar = 250 µm. **(B)** Survival of control and *stat2* disrupted zebrafish larvae 1-4 days post infection with *M. marinum*. p value was derived from a log-rank (Mantel-Cox) test. **(C-E)** Comparison of integrated fluorescence (IF) (a surrogate for bacterial burden) **(C)**, number of bacterial foci **(D)** and spatial distribution of bacteria **(E)**, in *stat2* CRISPants compared to control RNP injected siblings. Each data point represents an individual zebrafish larva, lines and error bars indicate the median and interquartile range. p values were derived from two-tailed Mann-Whitney tests. Data are representative of four experiments.

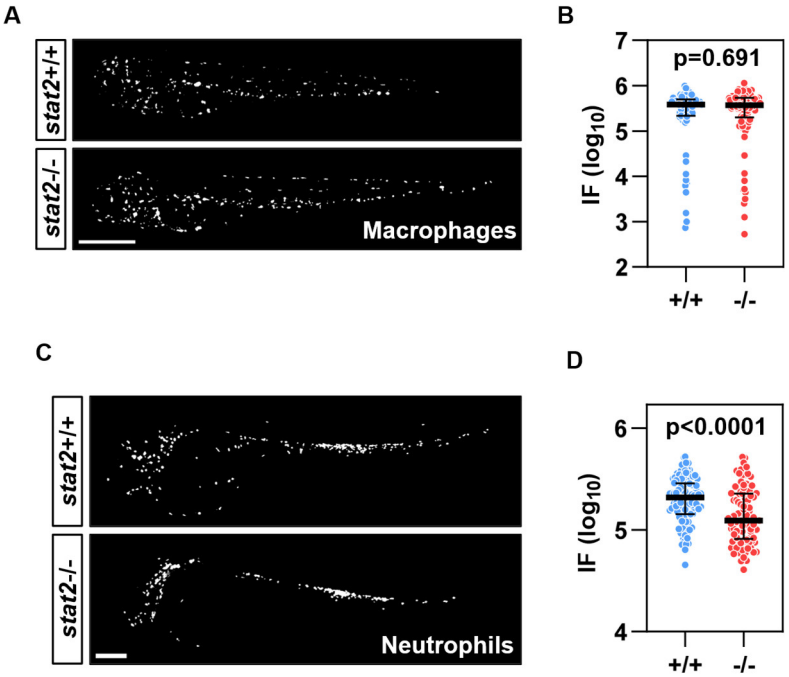

Fig. 4. Reduced steady state neutrophil numbers in *stat2* CRISPants. (A) Representative images of three day post-fertilisation (dpf) control (upper panel) and *stat2* CRISPant (lower panel) *Tg(mpeg1:mCherry)* zebrafish larvae. Scale bar = 250 μm. **(B)** Integrated fluorescence (IF) as a surrogate for steady state macrophage numbers in three dpf *stat2* CRISPants compared to siblings injected with scrambled RNPs. **(C)** Representative images of two dpf control (upper panel) and *stat2* CRISPant (lower panel) *Tg(mpx:eGFP)* zebrafish larvae. Scale bar = 250 μm. **(D)** Quantitation of baseline neutrophil numbers (represented by IF) in two dpf *stat2* CRISPants and negative control RNP injected siblings. Each data point represents an individual zebrafish larva, lines and error bars indicate the median and interquartile range. p values were derived from two-tailed Mann-Whitney tests. Data are from three independent experiments.

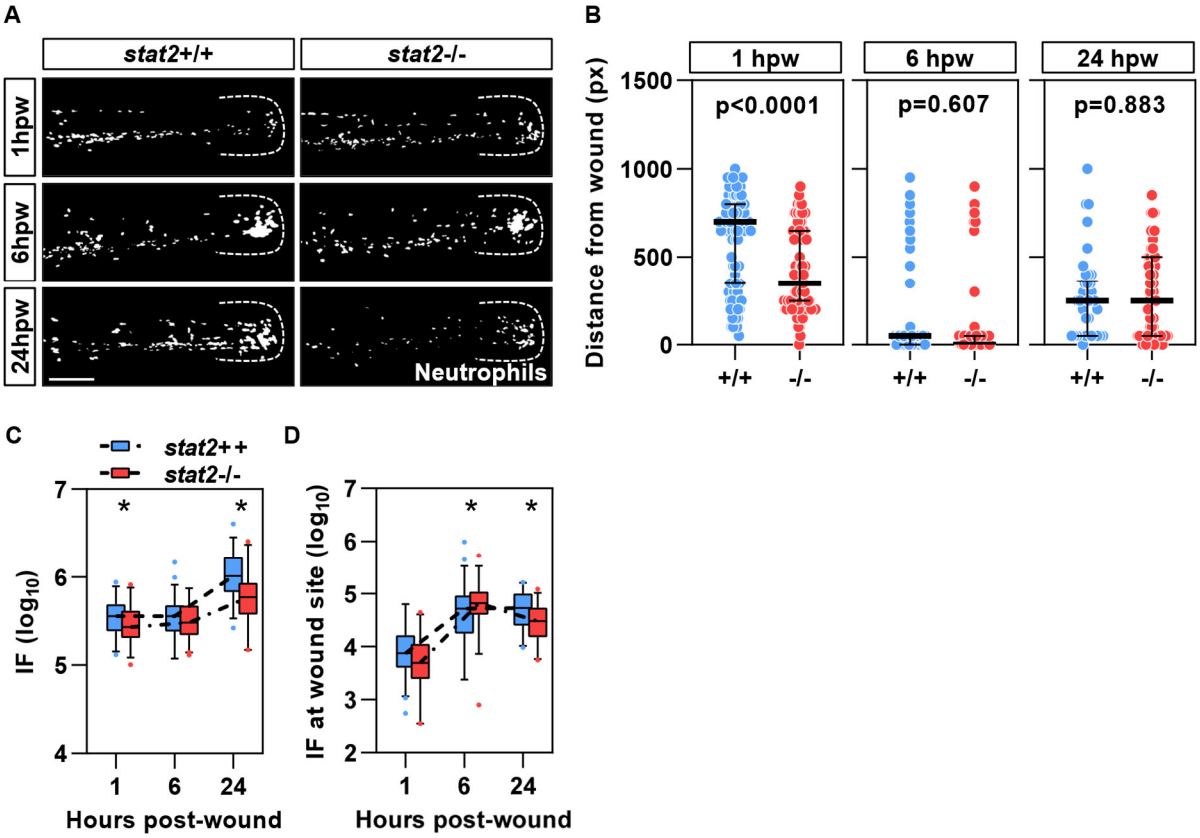

Fig. 5. Neutrophil recruitment to the site of sterile injury is not *stat2* dependent. **(A)** Representative images of eGFP-expressing neutrophils recruited to the site of injury 1, 6 and 24 hours following tailfin transection of three day post-fertilisation *stat2* CRISPant *Tg(mpx:eGFP)* zebrafish larvae and scrambled RNP injected controls. Scale bar represents 100 µm. **(B)** Distance of neutrophils from the injury site at 1, 6 and 24 hours post-wound (hpw), derived by identifying the Sholl circle in which the maximum integrated fluorescence (IF), a surrogate for highest cell numbers, was detected in *stat2* CRISPants and scrambled RNP injected siblings. **(C-D)** IF, a surrogate for total neutrophil numbers **(C)**, and IF at the wound site, representing neutrophil numbers localized to the tailfin transection **(D)** are shown at 1, 6 and 24 hours following injury. On scatter plots data points represent individual zebrafish larvae and lines and error bars the median and interquartile range. On box and whisker plots horizontal lines represent median values, box limits indicate the interquartile range and whiskers extend between the 5th and 95th percentiles. p values were derived from two-tailed Mann-Whitney tests. * = p<0.05. Data are from three independent experiments. px = Pixels.

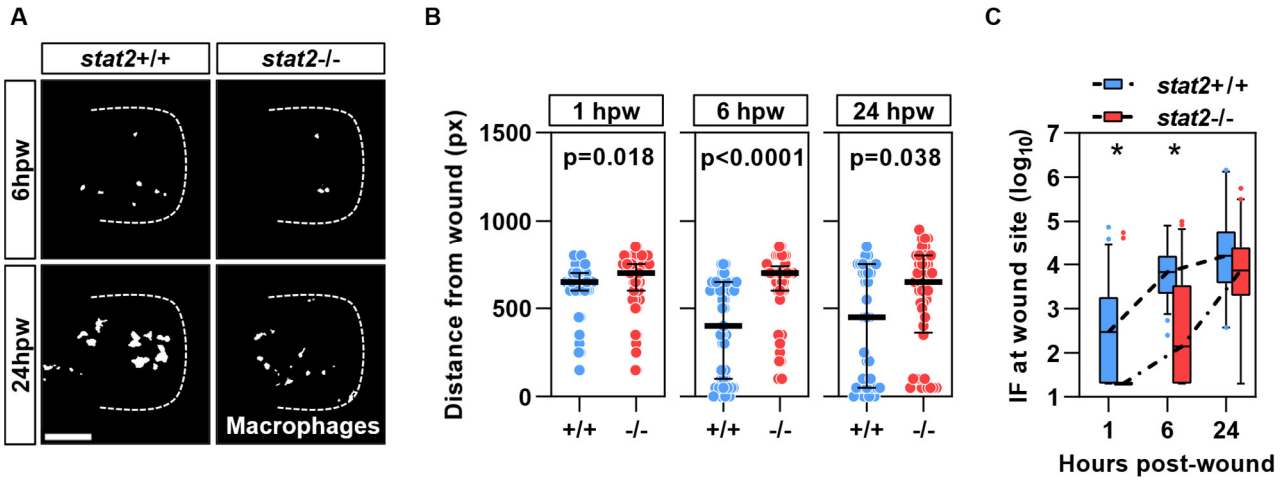

Fig. 6. Reduced macrophage recruitment to the site of sterile injury in *stat2* CRISPants. **(A)** Representative images of mCherry-expressing macrophages recruited to the site of tailfin transection by 6 and 24 hours, in three day post-fertilisation *stat2* CRISPant *Tg(mpeg1:mCherry)* zebrafish embryos and controls. Scale bar represents 100 μm. **(B)** Comparison of the distance of macrophages from the site of injury at the indicated time points for *stat2* CRISPants and control RNP injected siblings. **(C)** Integrated fluorescence (IF) a surrogate for macrophage numbers at the site of tailfin transection is shown at 1, 6 and 24 hours post-wound (hpw). On scatter plots data points represent individual zebrafish larvae and lines and error bars the median and interquartile range. On box and whisker plots horizontal lines represent median values, box limits indicate the interquartile range and whiskers extend between the 5th and 95th percentiles. p values were derived from two-tailed Mann-Whitney tests. * = p<0.05. Data are from three independent experiments. px = Pixels.

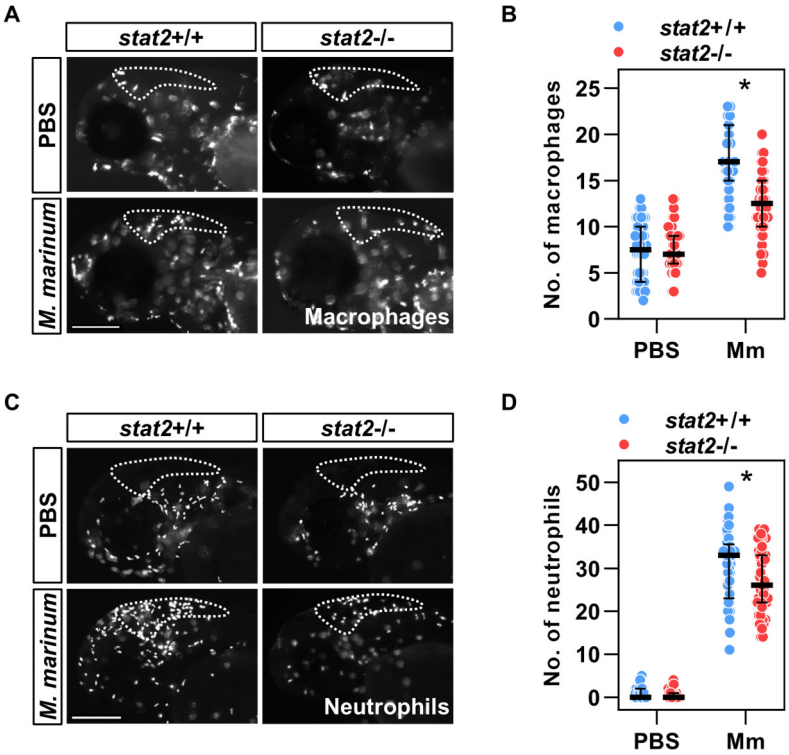

Fig. 7. Reduced macrophage and neutrophil recruitment to *M. marinum* in *stat2* CRISPants. **(A)** Representative images of mCherry-expressing macrophages recruited to the hindbrain (dashed white outline) 18 hours following injection of PBS or 200 colony forming units (cfu) *M. marinum* in two day post-fertilisation (dpf) *stat2* CRISPant *Tg(mpeg1:mCherry)* zebrafish larvae and scrambled ribonucleoprotein (RNP) injected controls. **(B)** Number of macrophages recruited to the hindbrain in response to PBS or *M. marinum* in *stat2* CRISPants and negative control RNP injected siblings. **(C)** Representative images of eGFP-expressing neutrophils recruited to the hindbrain 6 hours after PBS or *M. marinum* injection (200 cfu) in two dpf *stat2* CRISPant and control *Tg(mpx:eGFP)* zebrafish larvae. **(D)** Quantitation of neutrophils recruited to the site of *M. marinum* infection in *stat2* CRISPants and control siblings. Scale bars represent 100 μm. Data points represent individual zebrafish larvae and lines and error bars the median and interquartile range. p values were derived from two-tailed Mann-Whitney tests. * = $p<0.05$. Data are from three independent experiments.

TABLES

Table 1. Clinical and demographic data summary. Demographic characteristics and magnitude of clinical induration at the site of TST or saline injection are summarised for all study subjects. Duration of anti-tuberculous drug treatment at the time of sampling and radiographic disease severity data are provided for individuals with pulmonary TB. Saline samples were obtained from 17 individuals with pulmonary TB and 32 healthy participants who were people with cured or latent TB, BCG vaccine recipients and healthy volunteers, described previously *(8)*. CXR = chest x-ray. *Applies only to participants with active TB receiving saline injections.

		TST	Saline
Number		51	49
Age	(median and range)	30 (19-77)	28 (18-75)
Sex	Male	31 (61%)	19 (39%)
	Female	20 (39%)	30 (61%)
Ethnicity	White	21 (41%)	20 (41%)
	Asian	15 (29%)	8 (16%)
	Black	12 (24%)	7 (14%)
	Mixed	2 (4%)	1 (2%)
	South American	1 (2%)	11 (22%)
	Not recorded	NA	2 (4%)
Injection site induration (mm)	(median and range)	20 (0-70)	0
Days TB treatment before TST +/ saline	(median and range)	19 (0-30)	15 (0-28)*
CXR severity score	(median and range)	30 (0-140)	15 (0-110)*